6.10

EVALUATION OF THE ASR-9 WEATHER REFLECTIVITY PRODUCT*

Mark E. Weber
M.I.T. Lincoln Laboratory
Lexington, Massachusetts

John R. Anderson
University of Illinois
Urbana, Illinois

1. INTRODUCTION

The ASR-9 is a modern airport surveillance radar (ASR) under procurement by the United States Federal Aviation Agency. The radar operates at S-band, providing range-azimuth position information on aircraft targets within a 111-km radius. A fully-coherent klystron amplifier, large dynamic range and digital signal processing enable high integrity target processing and display under conditions of ground clutter, weather, angel clutter, RF interference and ground vehicular traffic (Taylor and Brunins, 1985; Karp and Anderson, 1981). To aid controllers in the identification of hazardous weather conditions, the processor will also generate two- or six-level weather reflectivity contours for display at the terminal radar control center and (potentially) remote sites.

In this paper, we present an overview of the ASR-9 and its weather processor, emphasizing those features that raise issues with respect to the utility of the weather reflectivity product in an air-traffic control environment. We then describe a simulation procedure that utilizes pencil-beam Doppler weather radar data and ground clutter measurements to preview the ASR-9 product and assess the effects of the radar's configuration on the weather intensity reports. Examples of the simulated weather reports are used to illustrate: (a) partial beamfilling due to the fan-shaped surveillance antenna pattern; (b) attenuation of low velocity weather by the clutter filters; (c) the effects of the spatial filters used in weather processing.

2. WEATHER CHANNEL DESCRIPTION

Table I summarizes parameters of the ASR-9's transmitter, receiver and antenna. The broad vertical beam and high antenna rotation rate are dictated by the need for detection and tracking of aircraft targets in terminal-area airspace. Many of the remaining parameters--for example, frequency, pulse-width, peak power, P.R.F. and A/D word size are consistent with the requirements for modern Doppler weather radar.

*The work described here was sponsored by the Federal Aviation Administration. The United States Government assumes no liability for its content or use thereof.

Two receiving beams ("high" and "low") are employed in a range-azimuth gated mode to mitigate the effects of ground clutter at short range. The feedhorns are mounted respectively below and above the focal axis of the antenna to produce beam response maxima at 6.5 and 2.0 degrees for a typical antenna tilt. One-way -3dB beamwidths are 4.8° minimum in elevation and 1.3° minimum in azimuth. The low beam is used for transmitting and for receiving at ranges beyond about 25 km. For receiving at shorter ranges the high beam is employed (the beam switching range is programable). Figure 1 shows the altitude of the patterns' -3dB points as a function of range. For reference, the coverage of a 1-degree pencil beam as would typically be used for weather radar is indicated by shading.

Consonant with the radar's beam pattern and pulse duration, target resolution space consists of 256 azimuth sectors (1.4 degrees) and 960 range gates (0-111 km at 0.116 km increments). During the time in which the antenna scans one azimuth sector, transmissions for an eight- and a ten-pulse coherent processing interval (CPI) occur. Within each CPI the interpulse period is fixed, but the interpulse periods of the two CPIs are different to prevent blind speeds and to provide discrimination against second-trip weather echoes. Transmissions of each CPI-pair are synchronized to antenna azimuth to allow stable geographic maps of clutter intensity to be constructed. These maps are used to control false alarms in the target processor and to select appropriate clutter filters in the weather channel.

The radar transmits either linearly or circularly polarized signals, selected according to air-traffic control requirements. Typically, linear polarization would be employed in clear weather or light precipitation. When echoes exceeding roughly 30 dBZ are present over a significant fraction of the radar's aerial coverage, a switch to circular polarization would take place to maintain tracking of aircraft targets.

Figure 2 is a block diagram of the six-level weather processing channel. An alternate two-level weather function, included as an integral part of the target processor, will not be described separately here.

During operation with circular polarization, the weather processor receives its input from the separate, orthogonal antenna port that does not attenuate echoes from spherical hydrometeors. In this mode, the high/low beam selection and sensitivity time control (STC) function can be set according to weather sensing requirements. During operations with linear polarization the weather channel's input is from the target channel A/D convertors and is therefore subject to the operating parameters selected for aircraft surveillance. The dynamic range of the processor is sufficiently large that neither clipping nor excessive attenuation of weather echoes due to inappropriate STC will pose a severe problem; however, the use of the high receiving beam to ranges as great as 30 km will significantly reduce the radar's ability to observe shallow, low-level weather hazards.

For each CPI, the input time series are passed through a bank of four finite impulse response clutter filters. One of the filters is all-pass whereas the other three are high pass with increasingly severe rejection of the scan-modulated ground clutter spectrum. Owing to the small number of filter coefficients, the stop- and transition bands of the high-pass filters will extend over a velocity interval that is significant for the detection of weather. For example, a filter achieving -40 dB clutter rejection will result in substantial attenuation for weather with radial velocity of 9 m/s or less.

To minimize such errors, a site-specific "clear-day" map of clutter intensities is maintained to enable the selection of the most appropriate clutter filter output for each weather level. The resolution of the map is 1.9 km by 1.4 degrees. In cells where the most severe filter cannot suppress ground clutter below one or more of the weather thresholds, the map enables censoring of weather detections for those levels.

Six weather thresholds are established to correspond to the National Weather Service levels of 0,30,41,46,50 and 57 dBZ. The threshold map allows the reflectivity estimates to be corrected for range, signal polarization and the high or low beam selection. Thus for example, corrections for STC differing from R^{-2}, or for partial beamfilling at long ranges can be made.

If a threshold is exceeded in half of the 16 range gates within a 1.9 km (1 n.mi.) interval, a weather detection is declared. The highest uncensored weather detection (or a censor flag) is output to the smoothing and contouring processor. The thresholding is repeated at 0.9-km increments for each of the 256 azimuth sectors.

Temporal smoothing is performed using three sequential reflectivity level estimates (accumulated over six antenna scans). The median level of the scans is computed to eliminate, for example, anomalously high returns in a single scan caused by a transient clutter source. A two-stage spatial filter incorporates data from the eight nearest-neighbor cells to minimize "holes" in the map due to clutter censoring and to smooth the weather contours for display.

3. SIMULATION OF THE WEATHER REFLECTIVITY PRODUCT

To evaluate the ASR-9's performance as a weather sensor, we have developed a computer simulation that utilizes pencil-beam Doppler weather radar data and ground clutter measurements at example U.S. airports. The simulation allows the each storm case to be "viewed" by an ASR-9 at arbitrary ranges and aspect angles. It allows for adjustment of weather parameters (e.g. mean velocity, spectrum width) as well as the radar operating configuration (e.g. beam-switching range, clutter filter selection) to facilitate an understanding of the relations between the radar's intrinsic resolution, the specified processing algorithms and the kinematics and morphology of a storm.

To facilitate translation of weather data in "range" and with respect to the clutter background, we first resample the reflectivity, velocity and spectrum width estimates onto a three-dimensional Cartesian grid. The grid spacing is chosen consistent with the resolution of the input products. After performing the appropriate coordinate transformations, data are sorted into ASR-9 weather channel range-azimuth cells (1.9 km by 1.4 degrees). For each cell, the reflectivity samples are weighted by the transmit and receive antenna pattern, integrated over elevation angle and normalized to produce the effective reflectivity factor as measured with a fan-shaped surveillance beam:

$$Z_{ASR}(R,\Phi) = \frac{\int_0^{\pi} Z(R,\Phi,\theta) B_T(\theta) B_R(\theta) d\theta}{\int_0^{\pi} B_R(\theta) B_T(\theta) d\theta} \qquad (1)$$

Reflectivity weighted radial velocity and spectrum width estimates are computed in an analogous manner.

Measured clutter cross-sections are integrated over each ASR-9 range azimuth cell. The radar range equation is used to compute the equivalent weather reflectivity factors, given the selected receiving beam. Three high-pass filters were constructed to achieve scan-modulated clutter attenuations of -12, -20 and -40 dB. The corresponding stop-band half-widths were 3, 5 and 9 m/s. As in the block diagram of Figure 2, one of the filters (or an all-pass characteristic) is selected for each range-azimuth cell and each weather level. Our criterion is to select the least attenuating filter that suppresses ground clutter 3 dB or more below the weather threshold. The ground clutter and weather reflectivities at the filter output are then computed, given the antenna scan rate and the weather radial velocity and spectrum width.

The variance of the resulting reflectivity field is small owing to the horizontal and vertical averaging employed. To simulate the statistical aspects of the ASR-9 processor we use the measured weather and clutter parameters to compute the weather threshold crossing probabilities for each resolution cell. The weather level "detected" for a single scan is then obtained

from a random number generator that conforms to the computed probability distribution.

If a resolution cell contains weather only, then the I and Q samples are independent Gaussian variables and the power estimate for a CPI is Gamma distributed (unnormalized Chi-squared). When both weather and ground clutter are present, the appropriate probability density function for the filter output power is a non-central Gamma distribution (Urkowitz, 1983). The parameters of these distributions are set by the (possibly filtered) weather and clutter reflectivities, and by the equivalent number of independent samples in a CPI. This last number may be computed from the weather spectrum width (Doviak and Zrnic, 1984). Note that in a single range-azimuth cell, different clutter filters may be selected for the different weather levels; for such cells, the parameters of the probability distributions are likewise level-dependent.

The single range-gate threshold crossing probabilities are determined by integrating these densities from a weather threshold to infinity. Designating the resulting threshold crossing probabilities by P(LEVEL) the threshold crossing probabilities at the output of the M-of-N detector are:

$$T(\text{LEVEL}) = \sum_{j=M}^{N} P(\text{LEVEL})^{j}\{1-P(\text{LEVEL})\}^{N-j}\frac{N!}{j!(N-j)!} \qquad (2)$$

Given these, the probability that a given weather threshold is the highest threshold crossed is:

$$Q(\text{LEVEL}) = T(\text{LEVEL})\cdot T(\overline{\text{LEVEL+1}},\ldots,\overline{6}\,|\,\text{LEVEL}) \qquad (3)$$

The second term on the right is the probability that none of the higher weather thresholds are exceeded, conditioned on the threshold "LEVEL" having been crossed. This is readily computed for the majority of the resolution cells where the different weather thresholds are compared against the same filter output (i.e., when ground clutter is not present). Where different clutter filters are invoked for different weather levels, these conditioned probabilities may be approximated by assuming that the outputs of the clutter filters are uncorrelated. (Two filter outputs will, of course, be partially correlated if the weather spectrum is non-zero where their passbands overlap. However, the magnitude of the resulting error in equation (3) is small, and does not affect the results reported here.)

The discrete inverse of the cumulative distribution function implied by equation (3) is applied to a uniformly distributed random number ($0 \leq X \leq 1$) to generate the "single-scan weather reports" at the M-of-N detector output. If the resulting level is censored, a flag is passed to the smoothing and contouring algorithms.

4. MEASUREMENTS

For the examples in this paper, weather radar data were obtained from the National Severe Storms Laboratory's "Norman" S-band radar. The case we consider was an intense squall line (maximum reflectivity 60 dBZ) that produced a well-defined gust front and turbulent downdrafts behind the front. Figure 3 shows the measured reflectivity, velocity and spectrum width fields at 2.3 degrees elevation. In this scan, the storm was centered 70 km west northwest of the radar, moving from 270 degrees. Note that the northern part of the developing gust front, as defined by the discontinuity in radial velocity and region of enhanced spectrum width, was directly beneath the storm's intense reflectivity volume whereas the southwards facing portion had begun to propagate away from the precipitation into low reflectivity air.

Ground clutter cross sections were measured with a Lincoln Laboratory X-band clutter measurement radar. The data displayed in this paper were obtained at the Dallas/Ft. Worth Airport, with the antenna height 15 meters, range resolution 300 meters and azimuthal beamwidth 0.9 degrees. Multiple frequency clutter measurements at Lincoln Laboratory indicate that, on the average, X-band clutter intensities and aerial extent are equal to those at S-band. Thus, while the data used here may not represent ASR-9 ground clutter on a cell-by-cell basis, they are a reasonable statistical approximation thereof. In the top two plots of Figure 4, these data have been used to compute areas where censoring would be necessary for weather levels 1 and 2 respectively. (In the examples in this paper, we will select the high receiving beam for ranges less than 28 km.) The third plot shows areas where the all-pass filter would be unsuitable, even for level 6 weather. It is seen that clutter censoring would not pose a significant problem for detection of level 3 weather or greater; however, as shown in the lower plot, filtering will be required for at least 7 percent of the radar's resolution space, with concomitant biases in the weather parameter estimates.

In Figures 5, we have used our simulation procedure to merge the weather and ground clutter measurements. For this example, the storm cells have been rotated 45 degrees and translated to a range of approximately 40 km with respect to the assumed ASR-9 position (indicated by the cursor). In this example, we have simply set the weather velocity everywhere equal to 16 m/s--representative of the measured radial velocities in the storm. The wind direction is from 225°, owing to the coordinate rotation. A constant 3 m/s weather spectrum width has been assumed.

Figure 5a, showing the sum of the vertically integrated weather power and the unfiltered ground clutter power, is indicative of the intrinsic capability of the fan-beamed radar. Owing to the height of the echoes in this storm the reflectivity values reported in cells without ground clutter are an accurate measure of the severity of the storm. Figure 5b displays the simulated output of the M-of-N detector in the ASR-9 processor. Censored range-azimuth cells are white in the display, and those cells where none of the weather thresholds were crossed are black. Note that while clutter censoring is significant in level 1 regions, the filters are generally effective in suppressing clutter for the higher levels. Attenuation of weather power by the clutter filters is also negligible, owing

to the high velocity of the weather. Figure 5c shows the output of the first stage spatial filter; this filter returns the highest detected weather level that is present in a specified fraction of a 9-cell nearest-neighbor cluster. It is reasonably effective in eliminating isolated threshold crossings and in filling in small "holes" due to clutter censoring. A second "contouring" algorithm returns the highest weather level in each 9-cell cluster, further smoothing the weather maps and increasing the area of the reported precipitation. The resulting output reflectivity product is displayed in Figure 5d.

In Figure 6 we have set the radial velocity of the weather everywhere to zero and moved the storm in towards the "radar". In the resulting map, attenuation of weather echoes by the ground clutter filters occurs, for example, in the areas designated by "A". Note also that the weather levels reported at some locations, for example "B", are one higher than the corresponding reports in Figure 5. This is an effect of vertical gradients in the reflectivity factor, which lead to a downward bias in the ASR-9 weather reports at longer ranges. Figure 7 plots the reflectivity factor profile at position "B". Also shown is the corresponding integrated reflectivity as sensed by a fan-beamed ASR-9, plotted as a function of range. In the low beam, the decrease at range of the vertically weighted reflectivity factor is 5 dB, accounting for the one-level drop in the output report.

5. DISCUSSION

While spatial and reflectivity-level resolution have obviously been reduced in the weather processor, the output product meets the air controllers' needs for a robust, easily interpreted indicator of the location and intensity of precipitation. Weather report biases due to partial beamfilling and attenuation of weather by the clutter filters occur but--for the severe storm treated here--their magnitude is not large. Future work will include similar analysis of a variety of storm types--severe storms, air-mass thunderstorms and stratiform precipitation. We anticipate that the analysis will contribute to the selection of site dependent processing parameters (e.g. high/low beam selection and reflectivity normalizations) and to planning for the utilization of the output product.

Information on storm velocity would be useful. In the example treated here, a developing gust front--clearly observable with the NSSL Doppler radar--had propagated as far as 12 km beyond the level 2 weather contour. No indication of this feature was discernable in the simulated ASR-9 weather reflectivity maps. To evaluate the potential for the ASR-9 as a Doppler weather sensor, we are conducting a parallel analysis and simulation program using measured data and numerical storm models. Key issues are: (a) the performance of the fan-beamed radar against shallow, low-level wind shears; and (b) low Doppler resolution resulting from the short CPIs. If the performance estimates warrant, a candidate weather processor upgrade to provide Doppler information will be implemented and tested.

REFERENCES

Doviak, R. J., and D. S. Zrnic, 1984: Doppler Radar and Weather Observations. Academic Press, 458 pp.

Karp, D., and J. R. Anderson, 1981: Moving Target Detector (Mod II) Summary Report. Final Report ATC-95 (FAA-RD-80-77). M.I.T. Lincoln Laboratory, Lexington, MA.

Taylor, J. W., and G. Bronins, 1985: Design of a New Airport Surveillance Radar (ASR-9). IEEE Proc., 73, 284-289.

Urkowitz, H., 1983: Signal Theory and Random Processes. Artech House, 715 pp.

Table 1

PARAMETER SUMMARY

TRANSMITTER	
Peak Power (nominal)	1.1 MW
Pulse Width (-3 dB)	1.03 μs
Radiated Frequency	2.7 - 2.9 GHz
Pulse Repetition Frequency	928 - 1321 Hz
RECEIVER	
Noise Figure	4.1 dB
Sensitivity	-108 dBm
A/D Converter	12 bit
ANTENNA (Minimum Parameters)	
Power Gain	
Low Beam	33.5 dB
High Beam	32.5 dB
Azimuth Beamwidth, Both Beams (-3 dB)	1.3 deg.
Elevation Beamwidth (-3 dB)	
Low Beam	4.8 deg.
High Beam	4.8 deg.
Rotation Rate	12.5 RPM

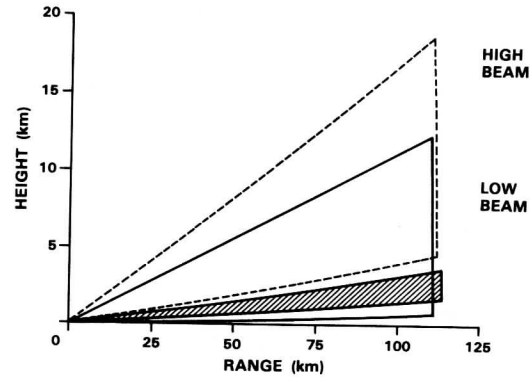

Fig. 1. Altitude limits vs range of the -3 dB points on the ASR-9 antenna patterns. The plot is for a 2.0-degree antenna tilt.

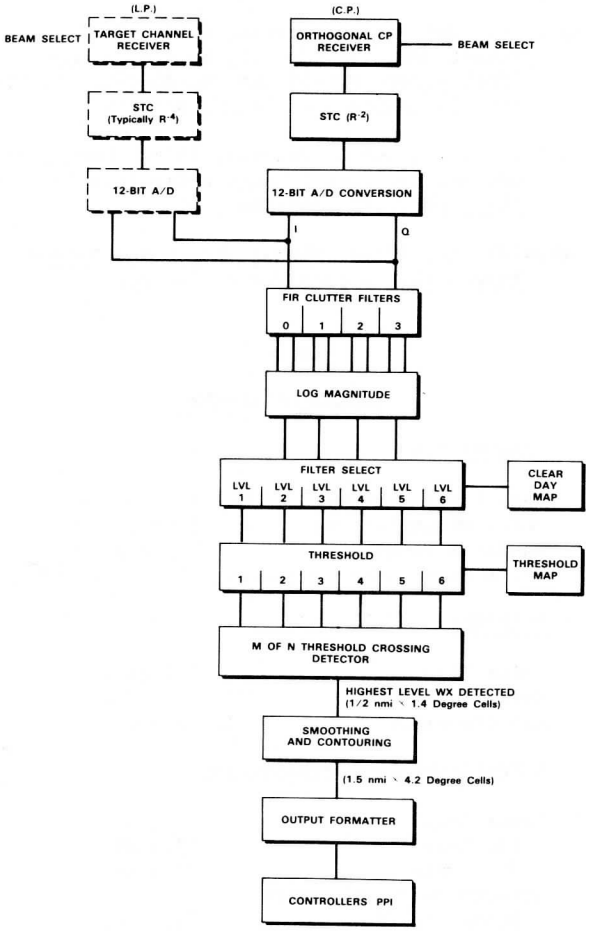

Fig. 2. Block diagram of six-level weather processor.

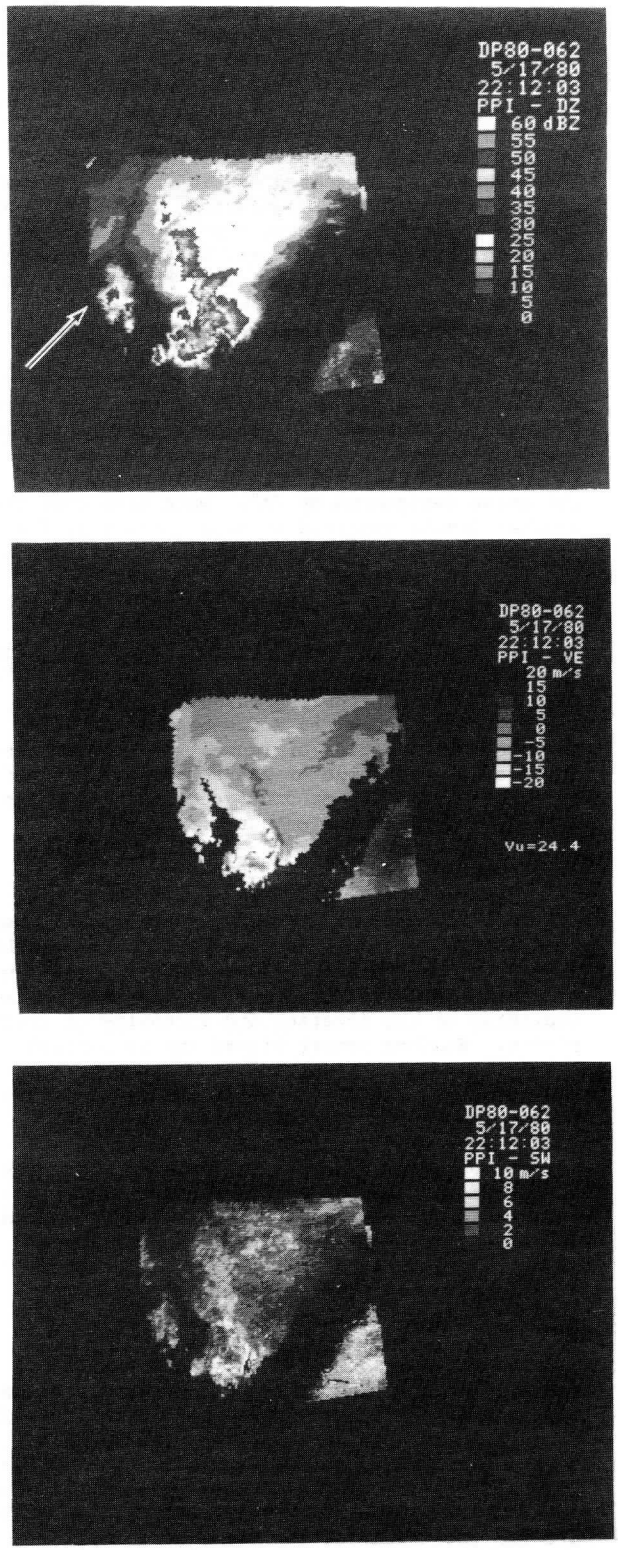

Fig. 3. PPI display of reflectivity factor mean radial velocity and spectrum width fields for severe storm near Norman, Oklahoma. Elevation angle is 2.3 degrees. The arrow indicates the placement of the "ASR-9" for the simulation in Figure 5.

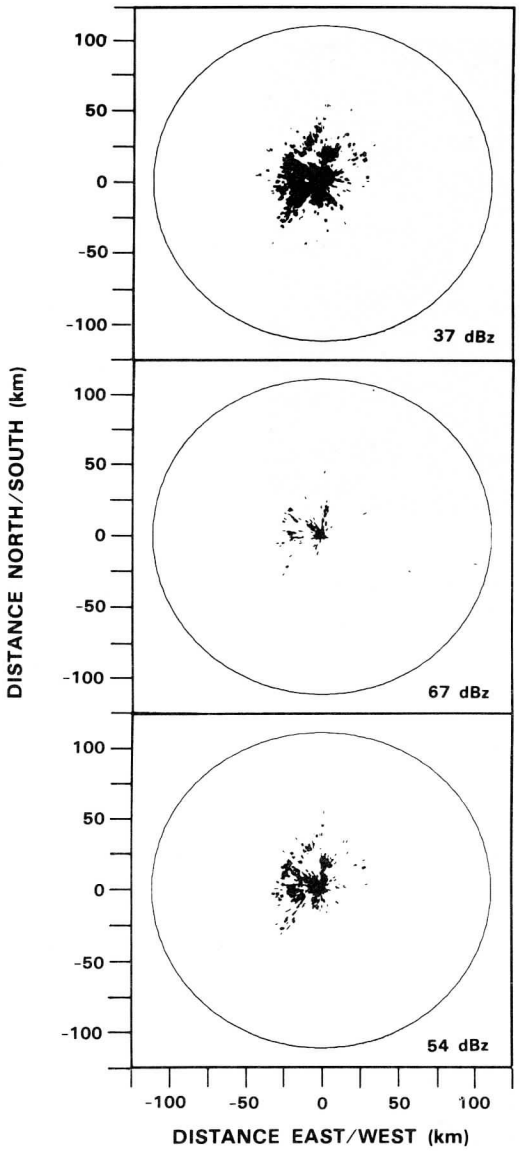

Fig. 4. Range-azimuth cells are darkened where the equivalent reflectivity factor for an ASR-9 radar at Dallas-Ft. Worth Airport would exceed the indicated thresholds.

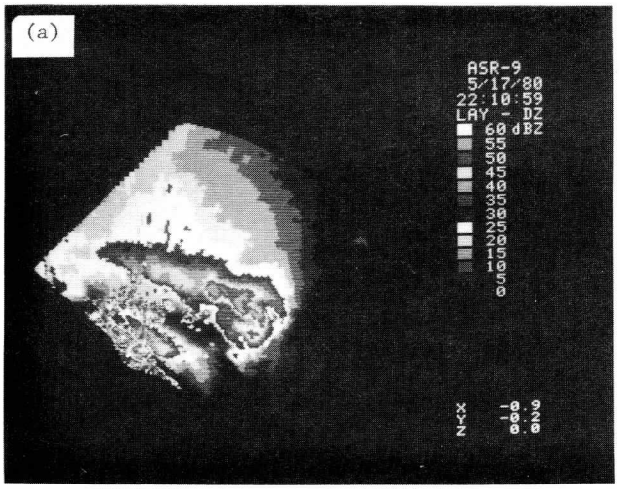

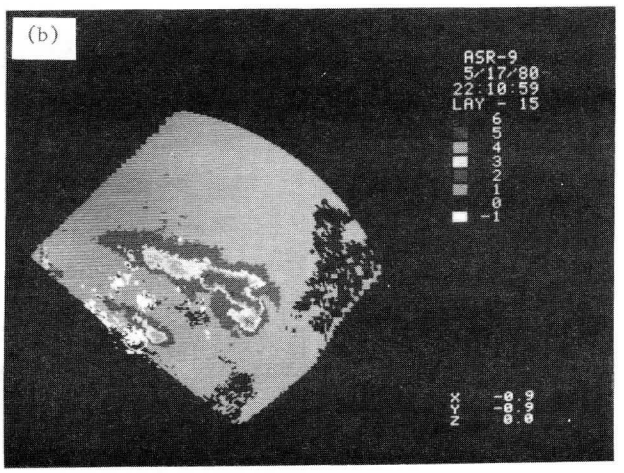

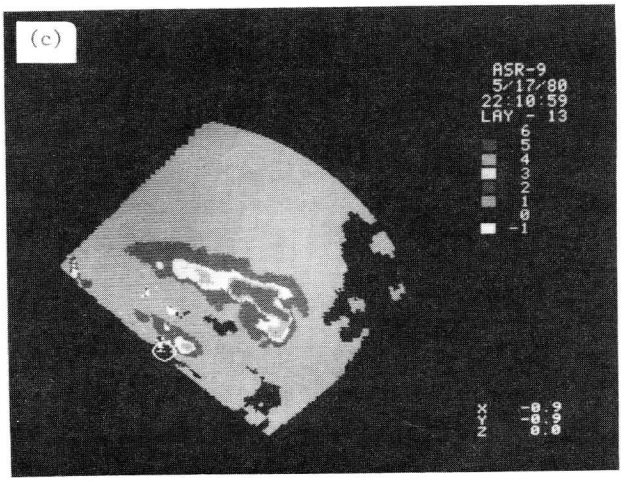

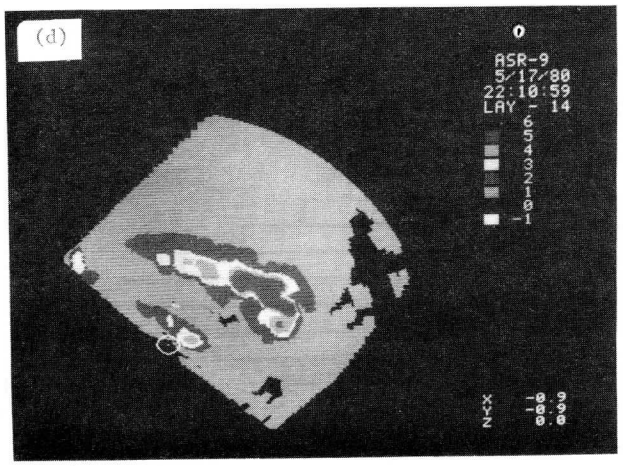

Fig. 5. Simulated ASR-9 weather reflectivity reports at various stages in the processing sequence.
(a) Elevation angle integrated weather reflectivity factor and equivalent clutter reflectivity in dBZ units.
(b) Output of the M-of-N detector.
(c) Output of the first-stage spatial filter.
(d) Output of the "contouring" processor.

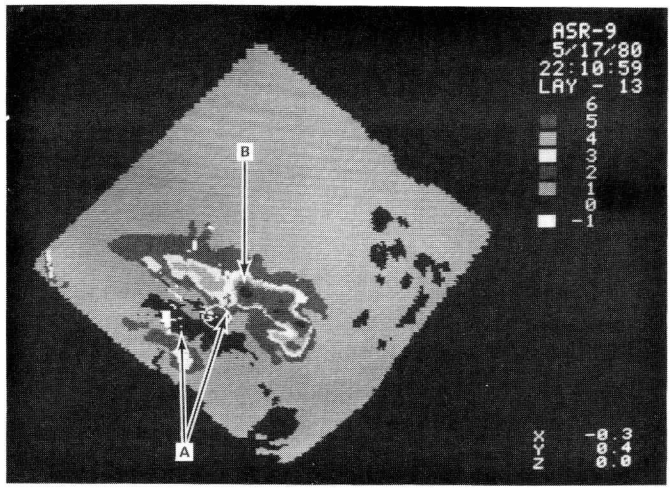

Fig. 6. Simulated output of the first-stage spatial filter for 0 m/s weather at short range from the radar. The areas designated by letters are as described in the text.

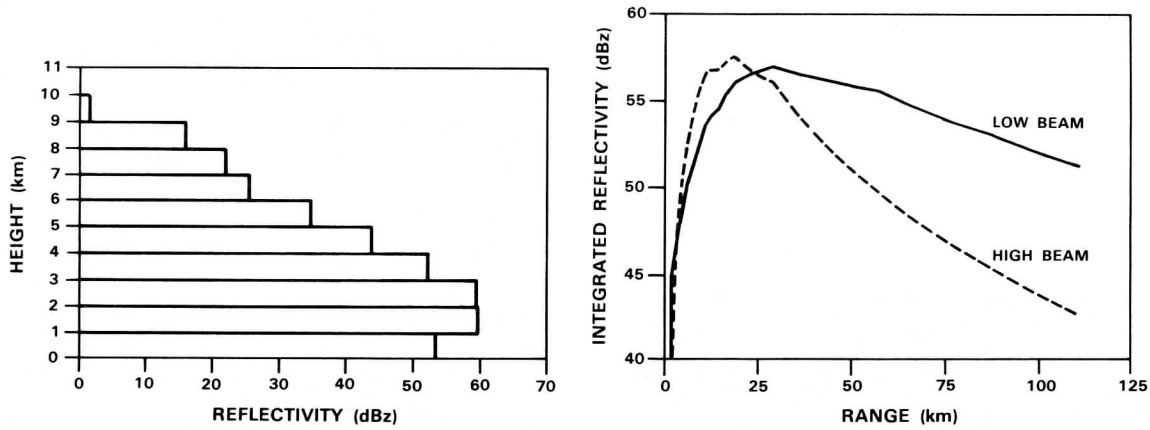

Fig. 7. (a) Profile of the reflectivity factor at the position indicated by "B" in Fig. 6.
(b) Corresponding elevation-angle-integrated reflectivity as sensed by an ASR-9; this is plotted as a function of range.